Chapter 3
Physically Based Stochastic Optimal Control

3.1 Preliminary Remarks

The notion of stochastic optimal control as currently defined has its roots in statistical methods for dealing with certain tracking and signal estimation problems arising from the existence of uncertainties inherent either in the measurement or in the excitation that drives the evolution of systems, which involve prediction, filtering, and data smoothing. The pioneering work on these problems was done by the mathematician Wiener, who is accredited as the founder of control theory (Wiener 1949). A large number of research efforts were devoted to estimation problems of practical interest in electronics, communications and control engineering. An important attempt was the filtering and prediction theory by Kalman and Bucy in the early 1960s (Bucy and Kalman 1961). Almost in the same period, the introduction of the state-space method (Kalman 1960a, b), the developments of the stochastic maximum principle (Kushner 1962), and the stochastic dynamic programming (Florentin 1961) in the context of Itô calculus received great attention. The stochastic optimal control theorem was then developed into a rather integrated system in the early 1970s (Åström 1970). Thereafter, the duality methods, as a major branch of the stochastic optimal control theory, also known as the Martingale approach, have been paid extensive attention in recent years because they offered powerful tools for the study of some classes of stochastic optimal control problems (Josa-Fombellida and Rincón-Zapatero 2007).

In the classical stochastic optimal control theory, the random disturbance specifying external excitations and measurement noise is typically assumed to be the additive white Gaussian noise or the filtered white Gaussian noise, and the pertinent schemes, such as the linear quadratic Gaussian (LQG) control and the covariance control, which aim to seek the optimal control gain in an admissible set by minimizing or maximizing the cost function of system state and control force (Stengel 1986). The application of the classical stochastic optimal control theory in the civil engineering has attained an extensive progress. For instance, Yang applied the LQG control into the active optimal control of engineering structures under random excitations

Y. Peng and J. Li, *Stochastic Optimal Control of Structures*,
https://doi.org/10.1007/978-981-13-6764-9_3

(Yang 1975). Chang and Yu developed an optimal pole assignment method in response to the vibration control of a single-degree-of-freedom system subjected to the white-noise excitation, i.e., using the control gain with the minimum variance, the pole of the closed-loop system could be transferred to the prespecified complex plane region (Chang and Yu 1998). Ho and Ma proposed a synthesis method combining the LQG and input estimation schemes, which was demonstrated to be better than the pure LQG control by a numerical simulation of active vibration control of lumped-mass systems (Ho and Ma 2007). Bani-Hani and Alawneh developed a set of posttensioning system with active prestress for the vibration control of bridges and utilized the LQG control in design of constant and variant control gains (Bani-Hani and Alawneh 2007). Kohiyama and Yoshida proposed a parameter design method for the LQG control so as to reduce the displacement and acceleration of computational facilities under the strong earthquakes (Kohiyama and Yoshida 2014).

The classical stochastic optimal control theory, however, implies an assumption of weak excitations in essence (Zhu 2006). Actually, as seen in the history of stochastic optimal control, the stochastic dynamics underlies its elementary substance, but the present theoretical frame of the stochastic dynamics is exclusively based on the white or filtered white noises and the Itô calculus (Lin and Cai 1995; Øksendal 2005). Therefore, the applicability of the classical stochastic optimal control theory in the vibration control of civil engineering structures still remains open since the practical excitations are nonstationary and non-Gaussian processes, such as seismic ground motions, high winds, and huge waves (Sun 2006). As an insight into this challenge, this chapter is devoted to developing a methodology of stochastic optimal control for response reduction of structures with actively closed-loop control systems, integrating the physically motivated random excitation model and the probability density evolution theory. The pertinent topics include the definition of control law of stochastic optimal control of structures using Pontryagin's maximum principle, the parameter design and optimization of controllers. Since the concern of the methodology lies upon the probability density evolution of structural systems during the control process, it is also referred to as the probability density evolution method (PDEM)-based stochastic optimal control.

3.2 Performance Evolution of Controlled Systems

As mentioned in the previous chapters, the probability density evolution method provides the theoretical foundation for the accurate analysis and design of stochastic dynamical systems. Naturally, this method can be extended to stochastic optimal control of stochastic dynamical systems so as to circumvent the dilemma that the classical stochastic optimal control confronted with.

Without loss of generality, the state equation of controlled systems subjected to random excitations is written as

$$\dot{\mathbf{Z}} = \boldsymbol{L}[\mathbf{Z}, \mathbf{U}, \boldsymbol{\Theta}, t] \tag{3.2.1}$$

where $\mathbf{Z}(t)$ is the $2n$-dimensional column vector denoting system state; $\mathbf{U}(t)$ is the r-dimensional column vector denoting control force; $\boldsymbol{\Theta}$ is the random vector characterizing the randomness inherent in the system; and $\boldsymbol{L}[\cdot]$ denotes the $2n$-dimensional vector of operator.

It is noted that the intervention of the control force necessarily affects the evolution trajectory of the system state, and the control force, on the contrary, needs to be regulated by the instantaneous system state in terms of the control law in feedback logic. In most cases, Eq. (3.2.1) is a well-posed equation and the system state $\mathbf{Z}(t)$ can be determined uniquely, which is a function of $\boldsymbol{\Theta}$ and might be assumed to take the following form:

$$\mathbf{Z}(t) = \mathbf{H}_{\mathbf{Z}}(\boldsymbol{\Theta}, t) \tag{3.2.2}$$

At the present stage, the explicit expression of the formal function $\mathbf{H}_{\mathbf{Z}}(\cdot)$ is not requisite and the sufficient condition is just its existence and uniqueness. Likewise, the control force $\mathbf{U}(t)$ is also a function of $\boldsymbol{\Theta}$ and can be assumed to take the following form:

$$\mathbf{U}(t) = \mathbf{H}_{\mathbf{U}}(\boldsymbol{\Theta}, t) \tag{3.2.3}$$

The velocities of $\mathbf{Z}(t)$ and $\mathbf{U}(t)$ can be thus assumed to take the following forms:

$$\dot{\mathbf{Z}}(t) = \mathbf{h}_{\mathbf{Z}}(\boldsymbol{\Theta}, t) \tag{3.2.4}$$

$$\dot{\mathbf{U}}(t) = \mathbf{h}_{\mathbf{U}}(\boldsymbol{\Theta}, t) \tag{3.2.5}$$

If the probability density function of a component of $\mathbf{Z}(t)$, denoted as $Z(t)$, without risk of confusion, is of interest, i.e.,

$$\dot{Z}(t) = h_Z(\boldsymbol{\Theta}, t) \tag{3.2.6}$$

The augmented system $(Z(t), \boldsymbol{\Theta})$ sustains a conservative probability since all the randomness involved in this system comes from $\boldsymbol{\Theta}$. There thus has

$$\frac{\mathrm{D}}{\mathrm{D}t} \int\limits_{\Omega_t \times \Omega_{\boldsymbol{\Theta}}} p_{Z\boldsymbol{\Theta}}(z, \boldsymbol{\theta}, t)\mathrm{d}z\mathrm{d}\boldsymbol{\theta} = 0 \tag{3.2.7}$$

where Ω_t, $\Omega_{\boldsymbol{\Theta}}$ are the distribution domain of t,$\boldsymbol{\Theta}$, respectively; $p_{Z\boldsymbol{\Theta}}(z, \boldsymbol{\theta}, t)$ is the joint probability density function of $(Z(t), \boldsymbol{\Theta})$. Through some mathematical manipulations, it follows (Li and Chen 2009)

$$\frac{\mathrm{D}}{\mathrm{D}t}\int\limits_{\Omega_t\times\Omega_{\boldsymbol{\Theta}}} p_{Z\boldsymbol{\Theta}}(z,\boldsymbol{\theta},t)\mathrm{d}z\mathrm{d}\boldsymbol{\theta}=\int\limits_{\Omega_t\times\Omega_{\boldsymbol{\Theta}}}\left(\frac{\partial p_{Z\boldsymbol{\Theta}}}{\partial t}+h_Z\frac{\partial p_{Z\boldsymbol{\Theta}}}{\partial z}\right)\mathrm{d}z\mathrm{d}\boldsymbol{\theta} \tag{3.2.8}$$

Combining Eqs. (3.2.7) and (3.2.8) and considering the arbitrary characteristics on the integral domain $\Omega_t\times\Omega_{\boldsymbol{\Theta}}$, we have

$$\frac{\partial p_{Z\boldsymbol{\Theta}}(z,\boldsymbol{\theta},t)}{\partial t}+\dot{Z}(\boldsymbol{\theta},t)\frac{\partial p_{Z\boldsymbol{\Theta}}(z,\boldsymbol{\theta},t)}{\partial z}=0 \tag{3.2.9}$$

Equation (3.2.9) is the so-called generalized probability density evolution equation (GDEE) for the augmented system $(Z(t),\boldsymbol{\Theta})$.

Likewise, for the component of control force $U(t)$, we have

$$\frac{\partial p_{U\boldsymbol{\Theta}}(u,\boldsymbol{\theta},t)}{\partial t}+\dot{U}(\boldsymbol{\theta},t)\frac{\partial p_{U\boldsymbol{\Theta}}(u,\boldsymbol{\theta},t)}{\partial u}=0 \tag{3.2.10}$$

The pertinent instantaneous PDFs of $Z(t)$ and $U(t)$ can be obtained by solving a family of partial differential equations with provided initial conditions as follows:

$$p_{Z\boldsymbol{\Theta}}(z,\boldsymbol{\theta},t)|_{t=0}=\delta(z-z_0)p_{\boldsymbol{\Theta}}(\boldsymbol{\theta}) \tag{3.2.11}$$

$$p_{U\boldsymbol{\Theta}}(u,\boldsymbol{\theta},t)|_{t=0}=\delta(u-u_0)p_{\boldsymbol{\Theta}}(\boldsymbol{\theta}) \tag{3.2.12}$$

where $\delta(\cdot)$ is the Dirac delta function; z_0,u_0 are determinative initial values of $Z(t)$, $U(t)$, respectively. We then have

$$p_Z(z,t)=\int\limits_{\Omega_{\boldsymbol{\Theta}}} p_{Z\boldsymbol{\Theta}}(z,\boldsymbol{\theta},t)\mathrm{d}\boldsymbol{\theta} \tag{3.2.13}$$

$$p_U(u,t)=\int\limits_{\Omega_{\boldsymbol{\Theta}}} p_{U\boldsymbol{\Theta}}(u,\boldsymbol{\theta},t)\mathrm{d}\boldsymbol{\theta} \tag{3.2.14}$$

where the joint PDFs $p_{Z\boldsymbol{\Theta}}(z,\boldsymbol{\theta},t)$ and $p_{U\boldsymbol{\Theta}}(u,\boldsymbol{\theta},t)$ are the solutions of Eqs. (3.2.9) and (3.2.10), respectively.

It is noted that the GDEE reveals the intrinsic relation of stochastic control system and deterministic control system via the realization of random vector $\boldsymbol{\theta}$, which underlies the realizability of probability-density-based optimal control for high-dimensional stochastic systems driven by practical nonstationary and non-Gaussian random excitations (Li and Chen 2008). One might recognize from Eqs. (3.2.9), (3.2.10), (3.2.13), and (3.2.14) that the kernel of implementing the probability-density-based optimal control is solving the physical quantity change $\dot{Z}(\boldsymbol{\theta},t)$, $\dot{U}(\boldsymbol{\theta},t)$ of systems with respect to the realization of random vector $\boldsymbol{\theta}$. Distinguished from the classical stochastic optimal control such as the LQG, the optimal control methodol-

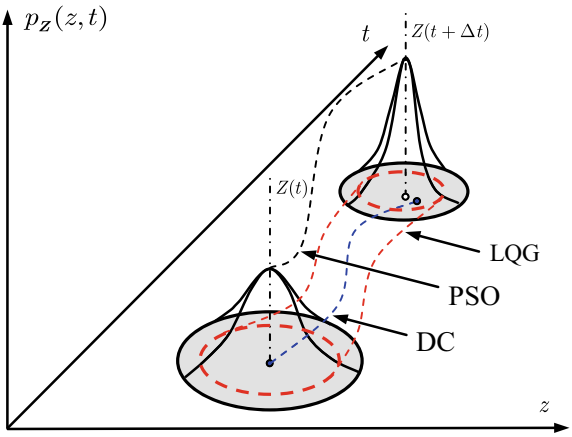

Fig. 3.1 Schematic of deterministic control (DC), LQG control, and physically based stochastic optimal (PSO) control

ogy on the basis of the GDEEs is termed as the physically based stochastic optimal control.

Figure 3.1 shows the differences from the deterministic control (DC), the LQG control, and the physically based stochastic optimal (PSO) control upon tracing the state evolution of controlled systems. It is ready to see that the trajectory of the deterministic control system is from point to point, which obviously lacks the ability of governing the system performance due to the randomness inherent in external excitations and measurement noise. The trajectory of the control system by the LQG is from circle to circle. It is noted that the classical stochastic optimal control is essentially a control scheme based on the second-order statistics, which just holds the system performance in the sense of mean-square quantities, and is incapable of attaining the complete probability information. The trajectory of the control system by the PSO, however, is from domain to domain, which can readily complement the accurate control of the system performance in the sense of probability density of quantities, owing to the advantage that the system quantities of interest are governed by the GDEEs, i.e., Eqs. (3.2.9) and (3.2.10).

3.3 Scheme of Stochastic Optimal Control

3.3.1 Closed-Loop Control Systems

Consider an n-degree-of-freedom linear structural system with active control devices and subjected to random excitations. The equation of motion is given by

$$\mathbf{M}\ddot{\mathbf{X}}(t) + \mathbf{C}\dot{\mathbf{X}}(t) + \mathbf{K}\mathbf{X}(t) = \mathbf{B}_s\mathbf{U}(t) + \mathbf{D}_s\mathbf{F}(\boldsymbol{\Theta}, t) \tag{3.3.1}$$

where $\mathbf{X}(t)$ is the n-dimensional column vector denoting system displacement; $\mathbf{U}(t)$ is the r-dimensional column vector denoting control force; $\mathbf{F}(\cdot)$ is the p-dimensional column vector denoting random excitations, which can be represented by a stochastic function in terms of the orthogonal decomposition of random processes (Li and Liu 2006) or introducing the physical mechanism of random processes (Li and Ai 2006); $\mathbf{M}$, $\mathbf{C}$, and $\mathbf{K}$ are $n \times n$ mass, damping, and stiffness matrices, respectively; $\mathbf{B}_s$ is the $n \times r$ matrix denoting the location of control devices; and $\mathbf{D}_s$ is the $n \times p$ matrix denoting the location of external excitations.

It should be noted that the random vector $\boldsymbol{\Theta}$ is considered to represent the randomness inherent in external excitations, and the measurement noise is ignored in this study since that the uncertainty arising from the measurement noise is more controllable compared with that arising from the random excitation. Meanwhile, although it is somewhat cumbersome, the notation $\boldsymbol{\Theta}$ underlies the fact that a random process is a function defined over the space of events of which $\boldsymbol{\Theta}$ is an element. Having noted this, the symbol $\boldsymbol{\Theta}$ would be dropped in the following development when the random nature of a certain quantity is obvious from the context except in the case of special denotation for a key quantity.

In the state space, Eq. (3.3.1) becomes

$$\dot{\mathbf{Z}}(t) = \mathbf{A}\mathbf{Z}(t) + \mathbf{B}\mathbf{U}(t) + \mathbf{D}\mathbf{F}(\boldsymbol{\Theta}, t) \tag{3.3.2}$$

with the initial condition

$$\mathbf{Z}(t_0) = \mathbf{z}_0 \tag{3.3.3}$$

where $\mathbf{A}$ is the $2n \times 2n$ system matrix; $\mathbf{B}$ is the $2n \times r$ matrix denoting the location of control devices, and $\mathbf{D}$ is the $2n \times p$ matrix denoting the location of external excitation, respectively,

$$\mathbf{Z}(t) = \begin{bmatrix} \mathbf{X}(t) \\ \dot{\mathbf{X}}(t) \end{bmatrix}, \mathbf{A} = \begin{bmatrix} \mathbf{0} & \mathbf{I} \\ -\mathbf{M}^{-1}\mathbf{K} & -\mathbf{M}^{-1}\mathbf{C} \end{bmatrix}, \mathbf{B} = \begin{bmatrix} \mathbf{0} \\ \mathbf{M}^{-1}\mathbf{B}_s \end{bmatrix}, \mathbf{D} = \begin{bmatrix} \mathbf{0} \\ \mathbf{M}^{-1}\mathbf{D}_s \end{bmatrix} \tag{3.3.4}$$

Equation (3.3.2) is numerically tractable using time integration methods, thereby any system quantities of interest such as displacement, velocity, acceleration, and control force can be readily derived.

The stochastic optimal control involves maximizing or minimizing a specified cost function. The generalized form of cost function is typically a quadratic combination of displacement, velocity, acceleration, and control force (Yang et al. 1994). Considering the linear quadratic regulator (LQR) as the control logic of the PSO, a standard quadratic cost function is given by (Soong 1990)

$$J_1(\mathbf{Z}, \mathbf{U}, \boldsymbol{\Theta}) = \frac{1}{2}\mathbf{Z}^{\mathrm{T}}(t_f)\mathbf{S}(t_f)\mathbf{Z}(t_f) + \frac{1}{2}\int_{t_0}^{t_f} [\mathbf{Z}^{\mathrm{T}}(t)\mathbf{Q}_{\mathbf{Z}}\mathbf{Z}(t) + \mathbf{U}^{\mathrm{T}}(t)\mathbf{R}_{\mathbf{U}}\mathbf{U}(t)]\mathrm{d}t \tag{3.3.5}$$

where $\mathbf{Q}_{\mathbf{Z}}$ is a $2n \times 2n$ positive semi-definite weighting matrix with respect to system state; $\mathbf{R}_{\mathbf{U}}$ is an $r \times r$ positive definite weighting matrix with respect to control force; t_0 is the initial time; and t_f is the terminal time which is usually larger than the duration of the external excitation. As should be noted, the cost function of the classical LQG is defined as ensemble average on the right terms of Eq. (3.3.5), which is a deterministic function; its minimization aims to attain the optimal gain with minimum cost under the assumption of white Gaussian noise as the external excitation and the given parameters of control law. In this case, the optimal gain relies upon second-order statistics of system quantities, which allows for a mean-square solution of control system, but the probability distribution of the system state pertaining to structural reliability is still unknown. The cost function of the PSO, i.e., Eq. (3.3.5), however, is a random function; its minimization aims to derive a stochastic optimal gain with parameters of control law of which the design and optimization through cost-effect analysis over realizations of random vector can attain the desired probability distribution of the system state. The proposed procedure is suitable for the optimal control of general stochastic systems, without assumption of white Gaussian noise as the external excitation.

In brief, the procedure involves a two-step optimization; see Fig. 3.2. In the first step, for each realization (sample) $\boldsymbol{\theta}$ of the random vector $\boldsymbol{\Theta}$, the minimization of the cost function Eq. (3.3.5) is carried out to build a functional mapping from the set of parameters of control law to the set of control gains. In the second step, the optimal parameters of control law to be used are obtained by optimizing the control gain as a probabilistic criterion pertaining to the structural performance objective.

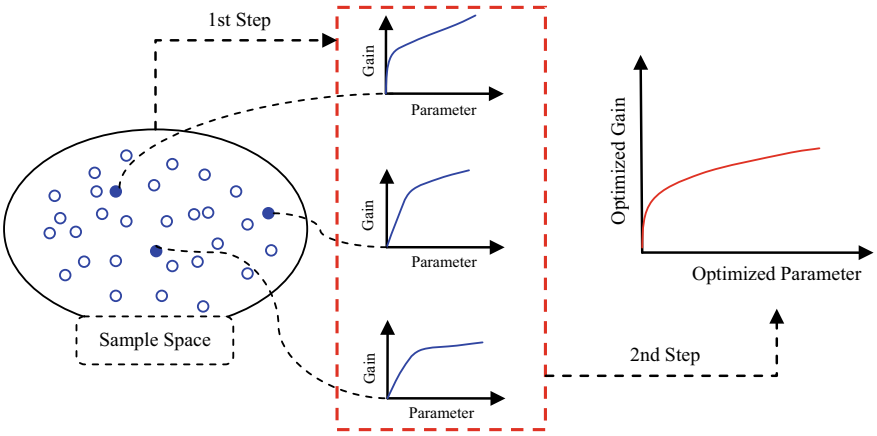

Fig. 3.2 Two-step optimization of physically based stochastic optimal control

Therefore, viewed from representative realizations, the minimization of the cost function J_1 leads to a conditional extreme-value problem. Introducing the costate vector $\boldsymbol{\lambda}(t) \in \mathbb{R}^n$ and utilizing the Lagrange multiplier method, we have

$$J_1(\mathbf{Z},\mathbf{U},\boldsymbol{\lambda},\mathbf{F},\boldsymbol{\Theta}) = \frac{1}{2}\mathbf{Z}^{\mathrm{T}}(t_f)\mathbf{S}(t_f)\mathbf{Z}(t_f) + \int_{t_0}^{t_f} [H(\mathbf{Z},\mathbf{U},\boldsymbol{\lambda},\mathbf{F},\boldsymbol{\Theta},t) - \boldsymbol{\lambda}^{\mathrm{T}}(t)\dot{\mathbf{Z}}(t)]\mathrm{d}t \tag{3.3.6}$$

where the Hamiltonian function is given by

$$H(\mathbf{Z},\mathbf{U},\boldsymbol{\lambda},\mathbf{F},\boldsymbol{\Theta},t) = \frac{1}{2}[\mathbf{Z}^{\mathrm{T}}(t)\mathbf{Q}_{\mathbf{Z}}\mathbf{Z}(t) + \mathbf{U}^{\mathrm{T}}(t)\mathbf{R}_{\mathbf{U}}\mathbf{U}(t)] + \boldsymbol{\lambda}^{\mathrm{T}}(t)[\mathbf{A}\mathbf{Z}(t) + \mathbf{B}\mathbf{U}(t) + \mathbf{D}\mathbf{F}(\boldsymbol{\Theta}, t)] \tag{3.3.7}$$

The necessary condition for the minimization of the cost function $J_1(\mathbf{Z},\mathbf{U},\boldsymbol{\lambda},\mathbf{F},\boldsymbol{\Theta})$ is deduced from the celebrated Pontryagin's maximum principle that the system state $\mathbf{Z}^*(t)$ denotes the optimal trajectory if the control force $\mathbf{U}^*(t)$ is referred to as an optimal control, and there must exist a costate $\boldsymbol{\lambda}^*(t)$ that allows for the Euler–Lagrange equation, as shown in Eqs. (2.2.13)–(2.2.15), in the presence of the random excitation. Then, we have

$$\frac{\partial H}{\partial \mathbf{U}} = \mathbf{R}_{\mathbf{U}}\mathbf{U}(t) + \mathbf{B}^{\mathrm{T}}\boldsymbol{\lambda}(t) = \mathbf{0} \tag{3.3.8}$$

which yields

$$\mathbf{U}(t) = -\mathbf{R}_{\mathbf{U}}^{-1}\mathbf{B}^{\mathrm{T}}\boldsymbol{\lambda}(t) \tag{3.3.9}$$

The costate equation Eq. (2.2.14) then turns to be

$$\dot{\boldsymbol{\lambda}}(t) = -\left(\frac{\partial H}{\partial \mathbf{Z}}\right)^{\mathrm{T}} = -\mathbf{Q}_{\mathbf{Z}}\mathbf{Z}(t) - \mathbf{A}^{\mathrm{T}}\boldsymbol{\lambda}(t) \tag{3.3.10}$$

As to a closed-open-loop control system with the state feedback and the input feedback simultaneously (Yang et al. 1987), the linear mapping between the costate $\boldsymbol{\lambda}(t)$ and the state $\mathbf{Z}(t)$, and the random excitation $\mathbf{F}(\boldsymbol{\Theta}, t)$ is deduced as (for the details; see Appendix B)

$$\boldsymbol{\lambda}(t) = \mathbf{P}(t)\mathbf{Z}(t) + \mathbf{S}_{\mathbf{F}}(t)\mathbf{F}(\boldsymbol{\Theta}, t) \tag{3.3.11}$$

where $\mathbf{P}(t)$, $\mathbf{S}_{\mathbf{F}}(t)$ are undetermined matrices with the terminal conditions

$$\mathbf{P}(t_f) = \mathbf{S}_{\mathbf{F}}(t_f) = \mathbf{0} \tag{3.3.12}$$

Substituting Eq. (3.3.11) into Eq. (3.3.9), one could obtain the control law

$$\mathbf{U}(t) = -\mathbf{R}_{\mathbf{U}}^{-1}\mathbf{B}^{\mathrm{T}}\mathbf{P}(t)\mathbf{Z}(t) - \mathbf{R}_{\mathbf{U}}^{-1}\mathbf{B}^{\mathrm{T}}\mathbf{S}_{\mathbf{F}}(t)\mathbf{F}(\boldsymbol{\Theta}, t) \tag{3.3.13}$$

Introducing Eq. (3.3.11) into Eq. (3.3.10) yields

$$\begin{aligned}&\dot{\mathbf{P}}(t)\mathbf{Z}(t) + \mathbf{P}(t)\dot{\mathbf{Z}}(t) + \dot{\mathbf{S}}_{\mathbf{F}}(t)\mathbf{F}(\boldsymbol{\Theta}, t) + \mathbf{S}_{\mathbf{F}}(t)\dot{\mathbf{F}}(\boldsymbol{\Theta}, t)\\ &= -[\mathbf{Q}_{\mathbf{Z}} + \mathbf{A}^{\mathrm{T}}\mathbf{P}(t)]\mathbf{Z}(t) - \mathbf{A}^{\mathrm{T}}\mathbf{S}_{\mathbf{F}}(t)\mathbf{F}(\boldsymbol{\Theta}, t)\end{aligned} \tag{3.3.14}$$

Namely,

$$\begin{aligned}&[\dot{\mathbf{P}}(t) + \mathbf{P}(t)\mathbf{A} + \mathbf{A}^{\mathrm{T}}\mathbf{P}(t) - \mathbf{P}(t)\mathbf{B}\mathbf{R}_{\mathbf{U}}^{-1}\mathbf{B}^{\mathrm{T}}\mathbf{P}(t) + \mathbf{Q}_{\mathbf{Z}}]\mathbf{Z}(t)\\ &= [\dot{\mathbf{S}}_{\mathbf{F}}(t) + \mathbf{A}^{\mathrm{T}}\mathbf{S}_{\mathbf{F}}(t) - \mathbf{P}(t)\mathbf{B}\mathbf{R}_{\mathbf{U}}^{-1}\mathbf{B}^{\mathrm{T}}\mathbf{S}_{\mathbf{F}}(t) + \mathbf{P}(t)\mathbf{D}]\mathbf{F}(\boldsymbol{\Theta}, t) - \mathbf{S}_{\mathbf{F}}(t)\dot{\mathbf{F}}(\boldsymbol{\Theta}, t)\end{aligned} \tag{3.3.15}$$

Equation (3.3.15) is the so-called differential Riccati equation and $\mathbf{P}(t)$ denotes the Riccati matrix.

It is indicated in Eq. (3.3.15) that the control law of a continuous time system involving the input feedback must be computed in real time according to the measured data since $\mathbf{P}(t)$, $\mathbf{S}_{\mathbf{F}}(t)$ are both coupled with $\mathbf{F}(\boldsymbol{\Theta}, t)$, $\mathbf{Z}(t)$. As mentioned previously, a critical task included in the proposed control scheme is the determination of probabilistic criterion, which relies upon the structural performance objective and naturally considers the influence of the random excitation. Therefore, the excitation-relevant term can be removed safely from the expression of control law. This treatment leads to a closed-loop control with the state feedback. The Riccati equation of the closed-loop control is then written as

$$\dot{\mathbf{P}}(t) = -\mathbf{P}(t)\mathbf{A} - \mathbf{A}^{\mathrm{T}}\mathbf{P}(t) + \mathbf{P}(t)\mathbf{B}\mathbf{R}_{\mathbf{U}}^{-1}\mathbf{B}^{\mathrm{T}}\mathbf{P}(t) - \mathbf{Q}_{\mathbf{Z}} \tag{3.3.16}$$

It is indicated in previous studies that the Riccati matrix $\mathbf{P}(t)$ remains the steady solution in a long interval after the initial time t_0, and comes into the transient solution rapidly until to zero near the final time t_f (Athans and Falb 1966). The starting time of the transient solution moves forward to t_f when the final time $t_f \to \infty$. Consequently, for the infinite-time control system, the Riccati matrix $\mathbf{P}(t)$ equals to its steady solution $\mathbf{P}$, and Eq. (3.3.16) thus becomes a matrix algebraic equation

$$\mathbf{P}\mathbf{A} + \mathbf{A}^{\mathrm{T}}\mathbf{P} - \mathbf{P}\mathbf{B}\mathbf{R}_{\mathbf{U}}^{-1}\mathbf{B}^{\mathrm{T}}\mathbf{P} + \mathbf{Q}_{\mathbf{Z}} = \mathbf{0} \tag{3.3.17}$$

According to Eq. (3.3.13), the control law of closed-loop control is thus given by

$$\mathbf{U}(\boldsymbol{\Theta}, t) = -\mathbf{G}_{\mathbf{Z}}\mathbf{Z}(\boldsymbol{\Theta}, t) \tag{3.3.18}$$

where $\mathbf{G}_{\mathbf{Z}}$ denotes the gain matrix of state-feedback control

$$\mathbf{G}_{\mathbf{Z}} = \mathbf{R}_{\mathbf{U}}^{-1}\mathbf{B}^{\mathrm{T}}\mathbf{P} \tag{3.3.19}$$

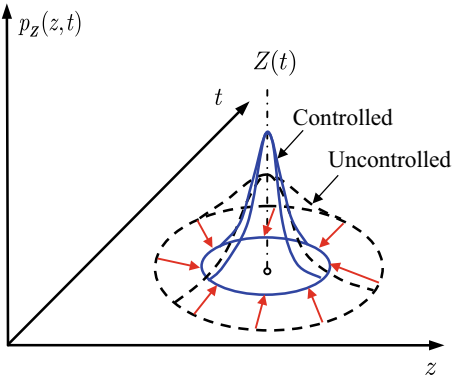

Fig. 3.3 Schematic of probability density of system state at typical instant of time with and without controls

Substituting the physical solutions of state quantity $\mathbf{Z}(t)$ and control force $\mathbf{U}(t)$ in the equation of motion of controlled structural system; see Eq. (3.3.2), into the generalized probability density evolution equations Eqs. (3.2.9) and (3.2.10), one can readily derive the probability density evolution process of system quantities of concern. Fig. 3.3 shows the schematic of probability density of system state at typical instant of time with and without controls.

3.3.2 Parameter Optimization of Control Law

The optimal control involves minimizing or maximizing a cost function in terms of system state and control force, either the deterministic cost function included in the classical LQG control or the stochastic cost function included in the proposed PSO control. The control effectiveness relies upon the derived control law pertaining to the structural performance objective. A critical step of designing control system is the determination of parameters of control law. It is seen from Eqs. (3.3.17)–(3.3.19) that the effort of designing the linear quadratic regulator (LQR) ought to be paid on the choice of cost-function weights $\mathbf{Q}_\mathbf{Z}$ and $\mathbf{R}_\mathbf{U}$. A number of strategies for the choice of cost-function weights were developed in the context of the classical LQG, such as the statistical moment evaluation based on the mathematical expectation of quantities of interest (Zhang and Xu 2001), the system robustness analysis in the sense of optimal probability (Stengel et al. 1992), and the weighting matrices comparison in the context of Hamiltonian theoretical framework (Zhu et al. 2001). In the context of the PSO, a strategy for cost-function weights choice is developed which is referred to as the system second-order statistics evaluation (Li et al. 2010), where the pertinent performance function involving evaluation and constraint quantities is proposed as follows:

$$J_2 = \bigcup_{j=1}^{N} F[\tilde{W}_j] \Big| \bigcup_{k=1}^{M} \{F[\tilde{V}_k] \leq \tilde{V}_{k,\mathrm{con}}\} \tag{3.3.20}$$

where $\tilde{W}_j = \max_t[\max_i|W_{ji}(\boldsymbol{\Theta}, t)|]$ denotes the jth component of the equivalent extreme-value vector to be evaluated; $\tilde{V}_k = \max_t[\max_i|V_{ki}(\boldsymbol{\Theta}, t)|]$ denotes the kth component of the equivalent extreme-value vector used as the constraint; $\tilde{V}_{k,\text{con}}$ denotes the threshold of the kth constraint; and the hat "~" on symbols indicates the equivalent extreme-value vector (Li et al. 2007); $\cup$ denotes the union operator; N, M denote the number of evaluation and constraint quantities, respectively; and $F[\cdot]$ is the quantile function denoting confidence level.

Therefore, the probabilistic criterion in terms of the system second-order statistics evaluation is defined as follows:

$$\{\mathbf{Q}_{\mathbf{Z}}^*, \mathbf{R}_{\mathbf{U}}^*\} = \arg\min_{\mathbf{Q}_{\mathbf{Z}}, \mathbf{R}_{\mathbf{U}}}\{J_2\} \tag{3.3.21}$$

The employment of the probabilistic criterion of Eq. (3.3.21) aims to seek the optimal cost-function weights $\mathbf{Q}_{\mathbf{Z}}^*$, $\mathbf{R}_{\mathbf{U}}^*$, under the condition of the quantile of the constraint less than its threshold, such that the quantile of the evaluation quantity is minimized. Herein, the evaluation quantity could be recognized as the extreme value of a structural response, e.g., interstory drift, interstory velocity, story acceleration, interstory shear force, and control force.

In this sense, the cost-function weights can be employed as (Soong 1990)

$$\mathbf{Q}_{\mathbf{Z}} = q\begin{bmatrix}\mathbf{I} & \mathbf{0}\\ \mathbf{0} & \mathbf{I}\end{bmatrix}, \mathbf{R}_{\mathbf{U}} = r\mathbf{I} \tag{3.3.22}$$

where q, r are coefficients of weighting matrices pertaining to system state and control force, respectively. The ratio between the two coefficients denotes the trade-off between the effect (mitigation ratio) and the cost.

It is worth noting that the abovementioned procedure underlies a heuristic algorithm of defining the cost-function weights $\mathbf{Q}_{\mathbf{Z}}$ and $\mathbf{R}_{\mathbf{U}}$. The details of the procedure will be presented in the numerical examples as shown in the following section.

3.4 Numerical Examples

3.4.1 Controlled Single-Story Building Structure

A planar single-story shear frame attached with an active tendon system as sketched in Fig. 3.4 is considered here, which is subjected to the horizontal random seismic ground motion $\ddot{x}_g(\boldsymbol{\Theta}, t)$. The properties of the system are as follows: the mass of the story is $m = 1 \times 10^5$ kg; the circular frequency of the uncontrolled structural system is $\omega_0 = 11.22$ rad/s; the control force of the actuator is denoted by $f(t)$; α represents the inclination angle of the tendon with respect to the base and the acting force $u(t)$

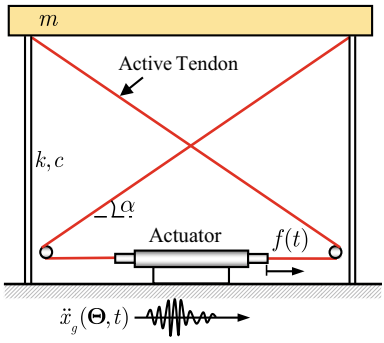

Fig. 3.4 Sketch of single-story shear frame with active tendon system

on the structure is simulated; and the damping ratio is set as 0.05. The interstory drift is considered as the constraint and the evaluation quantities include the interstory drift, the story acceleration, and the control force. The quantile function is defined as mean plus three times of standard deviation of the equivalent extreme-value variables. The threshold of interstory drift is specified to be 10 mm. The stochastic optimal control aims to assure the structural safety through controlling the interstory drift, to accommodate the structural habitability through controlling the story acceleration, and to satisfy with the system workability through controlling the output of the active tendon. Numerical simulation of structural responses employs a transfer function method, i.e., the S-transform of linear time-invariant (LTI) systems (Mathews and Fink 2003).

The physically motivated random seismic ground motion model addressed in Sect. 2.5.1 is employed to represent the random seismic ground acceleration. The conditional ground motion pertaining to the background of seismic hazards is introduced such that the influences of seismic source and wave propagation can be integrated as the input at the bedrock. The local site is viewed as a single-degree-of-freedom system; see Fig. 3.5. The physical relation between the surface ground motion and

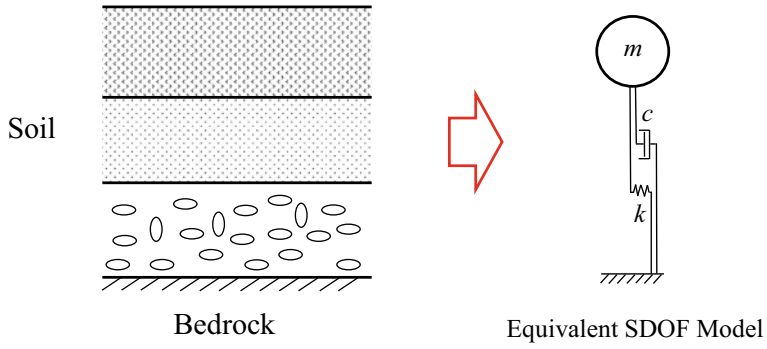

Fig. 3.5 Equivalent single-degree-of-freedom model of local site

bedrock ground motion, predominant circular frequency, and equivalent damping ratio of local site has a theoretical formulation as follows (Li and Ai 2006):

$$\ddot{X}_g(\boldsymbol{\Theta}, \omega) = \frac{\Theta_{\bar{\omega}_0}^2 + 2i\Theta_{\bar{\zeta}}\Theta_{\bar{\omega}_0}\omega}{\Theta_{\bar{\omega}_0}^2 - \omega^2 + 2i\Theta_{\bar{\zeta}}\Theta_{\bar{\omega}_0}\omega} \cdot \ddot{U}_b(\boldsymbol{\Theta}_b, \omega) \tag{3.4.1}$$

where $\ddot{X}_g(\boldsymbol{\Theta}, \omega)$, $\ddot{U}_b(\boldsymbol{\Theta}_b, \omega)$ are the frequency-domain expressions of ground motions at the surface of engineering site and at the bedrock, respectively. The ground motion at the bedrock is mathematically assumed to be a band-limited white noise, of which the Fourier amplitude is defined based on the background of seismic hazards; $\boldsymbol{\Theta} = (\Theta_{\bar{\omega}_0}, \Theta_{\bar{\zeta}}, \boldsymbol{\Theta}_b)$ is the random vector characterizing the randomness inherent in the ground motion at the surface of engineering site, which is used to model the randomness inherent in systems, of which $\Theta_{\bar{\omega}_0}$, $\Theta_{\bar{\zeta}}$ are the elementary random variables denoting the uncertainty of the site soil, i.e., the predominant circular frequency of engineering site $\bar{\omega}_0$ and the equivalent damping ratio $\bar{\zeta}$; $\boldsymbol{\Theta}_b = \{\Theta_{b,i}\}_{i=1}^{s_b}$ is the random vector characterizing the randomness inherent in the ground motion at the bedrock coming from the properties of seismic sources and wave propagation; s_b denotes the number of random variables; ω is the circular frequency; and i is the imaginary unit.

The time history of the random ground motion then could be attained by the inverse Fourier transform:

$$\ddot{x}_g(\boldsymbol{\Theta}, t) = \frac{1}{2\pi}\int_{-\infty}^{\infty} \ddot{X}_g(\boldsymbol{\Theta}, \omega)\mathrm{e}^{\mathrm{i}\omega t}\mathrm{d}\omega \tag{3.4.2}$$

The local site is assumed to have the properties of site class III and exhibit seismic fortification intensity 8 in terms of the Chinese Code for Seismic Design of Building Structures (GB50011-2010). Following the basic principle of stochastic modeling, the probabilistic structures and distribution parameters of the elementary random variables, i.e., the predominant circular frequency $\bar{\omega}_0$ and the equivalent damping ratio $\bar{\zeta}$ can be derived by the data fitting of recorded seismic accelerations using the least squares method. Numerical results show that the predominate circular frequency $\bar{\omega}_0$ and the equivalent damping ratio $\bar{\zeta}$ both follow the lognormal distribution, of which the mean and coefficient of variation of $\bar{\omega}_0$ are 12 rad/s, 0.42, respectively; the mean and coefficient of variation of $\bar{\zeta}$ are 0.1, 0.35, respectively. Considering the seismic hazard with return period 50 years, i.e., frequently occurring earthquake and peak ground acceleration $0.11g$, the Fourier amplitude of ground motion at the bedrock is set as 0.20 m/s^2. Meanwhile, the initial phase angle in the inverse Fourier transform for simulating seismic ground accelerations is assumed to follow the normal distribution, of which mean and coefficient of variation are π, 1.2, respectively. Utilizing the tangent spheres method to carry out the partition of probability-assigned space, 221 representative points and the pertinent time histories of seismic ground accelerations are generated (Chen et al. 2007; Chen and Li

2008). Sampling frequency and duration of the simulated ground motions are 50 Hz, 20.48 s, respectively.

In order to reveal the nonstationary intensity of seismic ground motions, the following uniform modulation function is used (Li and Chen 2009):

$$f(t) = \begin{cases} t^2/4, & t \le t_a \\ 1, & t_a < t \le t_b \\ \mathrm{e}^{-0.8(t-t_b)}, & t_b < t \le T \end{cases} \tag{3.4.3}$$

where t_a and t_b are set as 2 s and 16 s, respectively and T denotes the duration of the ground motion.

Statistical moments of the random seismic ground acceleration are shown in Fig. 3.6. It is seen that the amplitude of the mean (approximate 0.06 m/s^2) is around 8% of the amplitude of the standard deviation (approximate 0.8 m/s^2), indicating that the physically motivated random ground motion model exhibits the property of zero mean. Time history of a representative seismic ground acceleration is shown in Fig. 3.7. It is recognized that the random seismic ground acceleration exhibits remarkable nonstationary behaviors both in temporal and frequency domains. Two recorded seismic ground accelerations from the same site class, labeled as EL270 and EMC90, are shown in Fig. 3.8, of which the peak ground acceleration (PGA) is scaled to $0.1g$. For comparative purposes, the acceleration response spectra of the random seismic ground motion, representative, and recorded seismic ground motions are pictured; see Fig. 3.9. It is shown clearly that the mean plus standard deviation of acceleration response spectrum derived from the random seismic ground motion accommodates the acceleration response spectra derived from the recorded seismic ground motion, indicating the moderation of the selected seismic ground motions and the rationality of the physically motivated random seismic ground motion model. This knowledge owes to the fact that the physically motivated random seismic ground

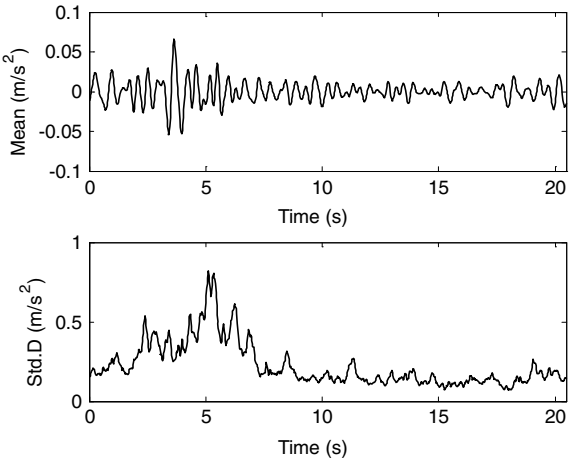

Fig. 3.6 Mean and standard deviation of random seismic ground acceleration

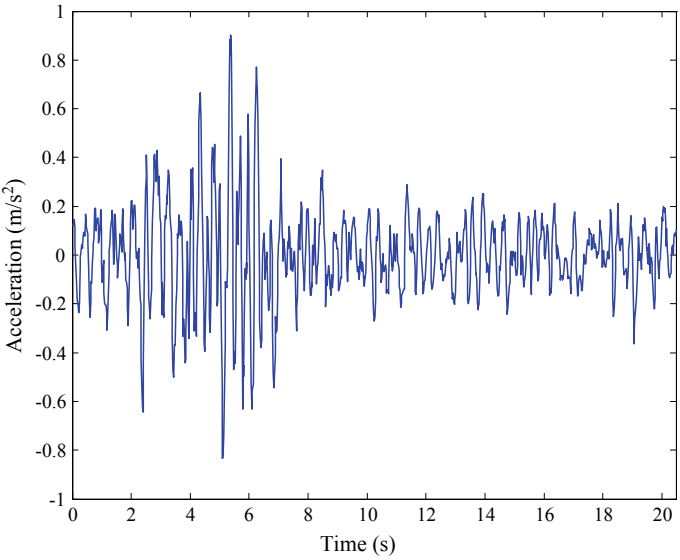

Fig. 3.7 Time history of representative seismic ground acceleration

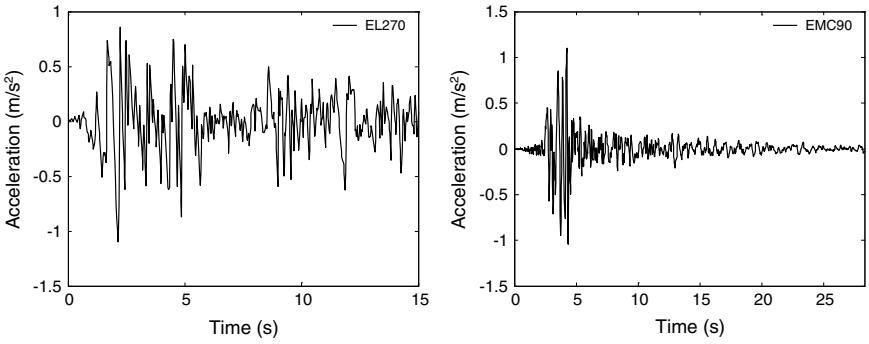

(a) EL270 (b) EMC90

Fig. 3.8 Time histories of recorded seismic ground accelerations from the same site class

motion model is a self-contained sample set with respect to simulated seismic ground motions; the selected seismic ground motions, in some sense, can be viewed as elements of another sample set of recorded seismic ground motions which has the same background of seismic hazards to the self-contained sample set.

In order to reveal the influence of cost-function weights on the stochastic optimal control, the relations between the equivalent extreme-value displacement, the equivalent extreme-value acceleration, the equivalent extreme-value control force, and the ratio of coefficients of weighting matrices q/r are presented in Fig. 3.10, where q is set as 100. It is clearly seen that these relation curves are different both from the

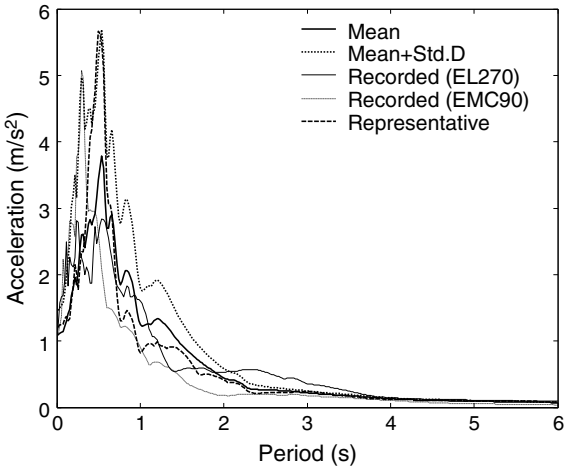

Fig. 3.9 Acceleration response spectra of random seismic ground motion, representative, and recorded seismic ground motions

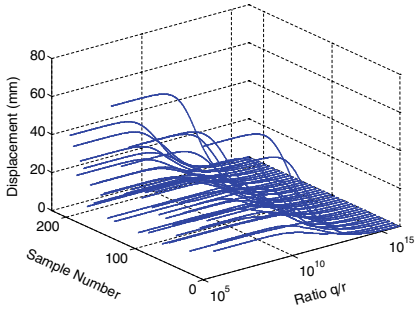

(a) equivalent extreme-value displacement

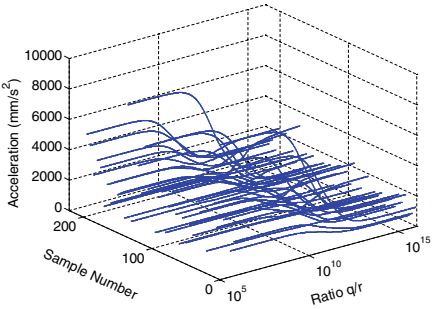

(b) equivalent extreme-value acceleration

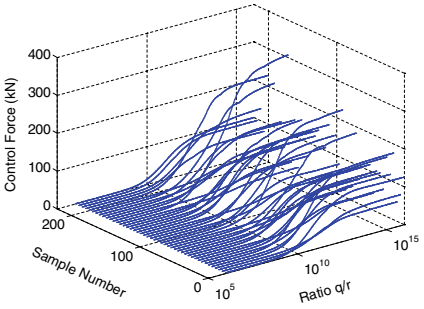

(c) equivalent extreme-value control force

Fig. 3.10 Relation between equivalent extreme-value quantities and ratio of coefficients of weighting matrices

structural responses and seismic ground motions, e.g., concerning the same seismic ground motion, the relation between control force and the ratio q/r changes from the structural displacement, velocity, and acceleration; concerning the same structural response, the relation between control force and the ratio q/r changes from seismic ground motions. The optimal ratio q^*/r^*, in other words, nominally arises to be different from samples of the random seismic ground motion and exhibits a certain randomness. Moreover, there exists a relevance between control effectiveness and control cost; the definition of the optimal ratio q^*/r^* shall consider the trade-off between system quantities of interest. One might wonder, however, which ratio of coefficients of weighting matrices for the stochastic optimal control exhibits the optimality in a global sense?

In fact, the control law involves a deterministic gain matrix even in the stochastic optimal control, which relies upon the structural performance objective and can be derived as a probabilistic criterion, e.g., the system second-order statistics evaluation. Figure 3.11 shows the relation between the mean of equivalent extreme -value displacement, equivalent extreme-value velocity, equivalent extreme-value

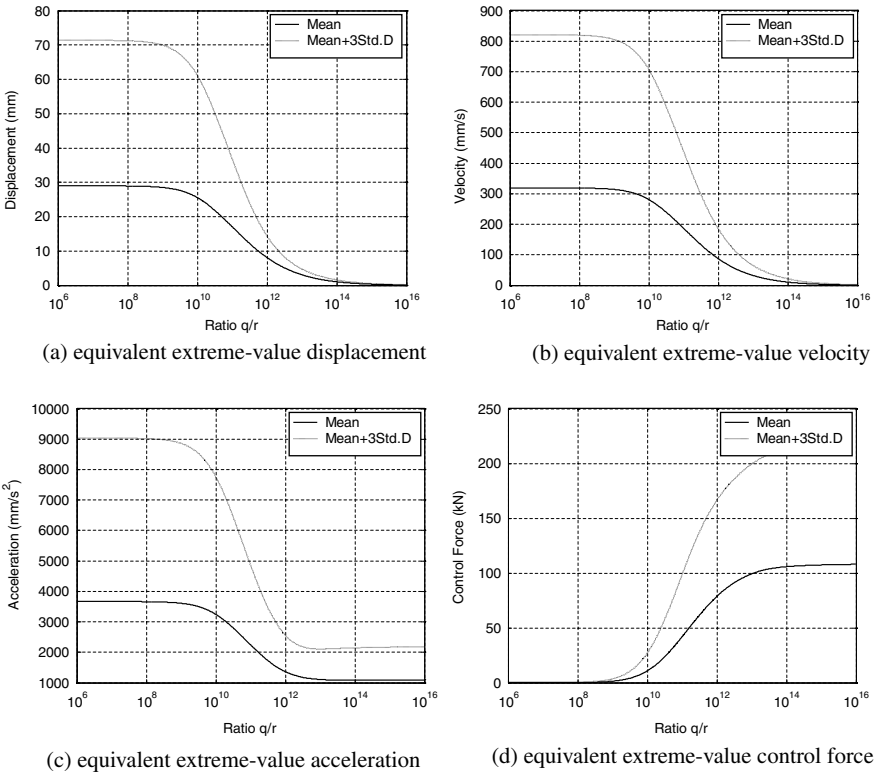

(a) equivalent extreme-value displacement

(b) equivalent extreme-value velocity

(c) equivalent extreme-value acceleration

(d) equivalent extreme-value control force

Fig. 3.11 Relation between mean, quantile of quantities, and ratio of coefficients of weighting matrices

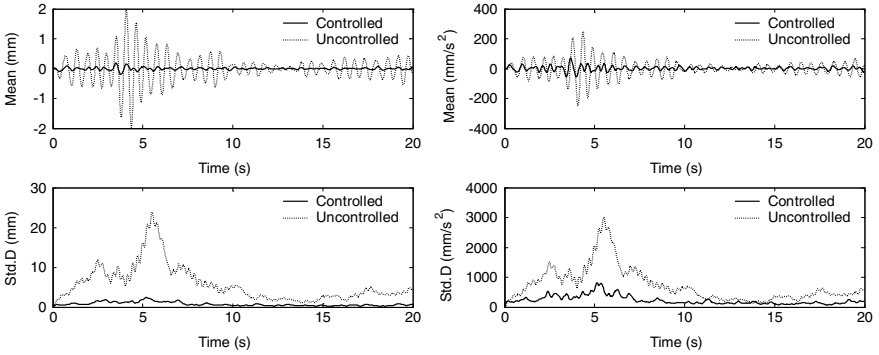

(a) structural displacement (b) structural acceleration

Fig. 3.12 Time histories of mean and standard deviation of structural responses with and without controls

acceleration, equivalent extreme-value control force, and the ratio q/r. The quantiles of these quantities are shown as well. It is seen that: (i) as ratio $q/r \geq 2\times 10^{12}$, the quantile of the displacement is completely within its threshold as a constraint; (ii) as ratio $q/r \geq 2\times 10^{14}$, the standard deviation of the displacement is minimum and the mean decreases slowly, whereas the standard deviation of the acceleration increases and the mean of acceleration decreases very gently; the mean and standard deviation of the control force, however, increase significantly; (iii) as ratio $q/r = 8\times 10^{12}$, the standard deviation of the acceleration attains minimum, although the standard deviation of the displacement is not minimum; meanwhile, the means of the acceleration and the displacement decrease evidently. The benefit at this ratio, moreover, lies in that the mean and standard deviation of the control force are much less than those at the ratio $q/r \geq 2\times 10^{14}$. Considering the trade-off between the quantities of interest, it is thus reasonable to take the optimal ratio $q^*/r^* = 8\times 10^{12}$; $q^* = 80$, $r^* = 10^{-11}$ in the numerical case.

Time histories of the mean and standard deviation of structural displacement and those of structural acceleration with and without controls are shown in Fig. 3.12. It is seen that the structural responses with control are reduced significantly in comparison with those without control. Moreover, the structural responses decrease significantly in the time interval with larger amplitudes; see the interval from 2 s to 8 s, which indicates that the stochastic optimal control aims at enhancing the structural robustness in a global sense. The amplitudes of standard deviations of the displacement and the acceleration with control are reduced by 5 and 3 times than those without control, respectively. It is also seen from Fig. 3.12 that the amplitude of the mean is around 8% smaller than that of the standard deviation. It is understood that the linear structural system is driven by the random seismic ground motion with zero mean.

Figure 3.13 shows the PDFs of the displacement of the controlled and uncontrolled structures at typical instants of time 4 s, 7 s, and 10 s. It is seen that the variation of the structural displacement with control is reduced significantly by comparison with

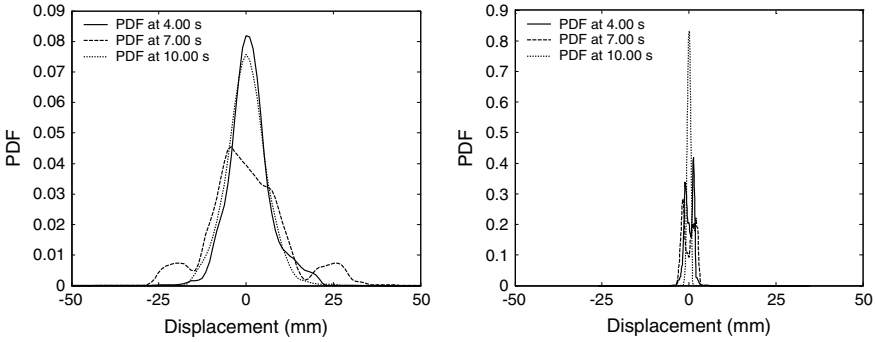

Fig. 3.13 PDFs of structural displacement at typical instants of time

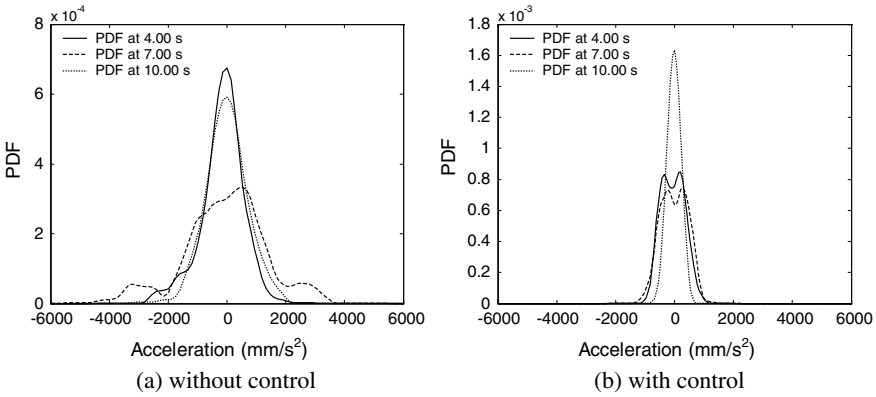

Fig. 3.14 PDFs of structural acceleration at typical instants of time

that without control. The PDFs of the structural acceleration at typical instants of time show similar properties to the structural displacement, as shown in Fig. 3.14. It is revealed that the seismic performance of the structure has been enhanced greatly after the stochastic optimal control is applied. For details of time-varying probabilistic information, the probability densities of structural displacement and structural acceleration at typical time interval from 4 s to 10 s are shown in Figs. 3.15 and 3.16, respectively.

The mean and standard deviation of control force and PDFs at typical instants of time are shown in Fig. 3.17. It is seen that the shapes of the mean and standard deviation of control force and the pertinent curves of the probability density function exhibit certain similarities to the structural displacement and structural acceleration. These similarities are resulted from the cause that the optimal control force is pursuing the structural response in real time, which is a weighted combination of structural displacement and velocity as the relevant elements of the gain matrix (Chung et al.

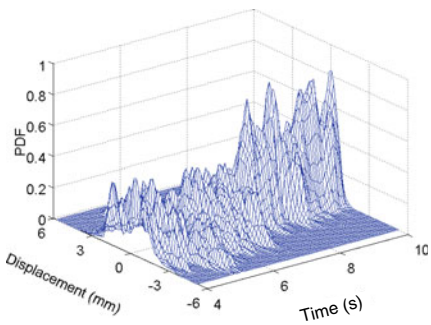

(a) probability density surface

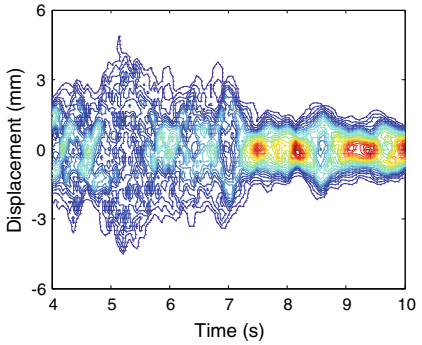

(b) probability density contour

Fig. 3.15 Probability density of structural displacement at typical time interval

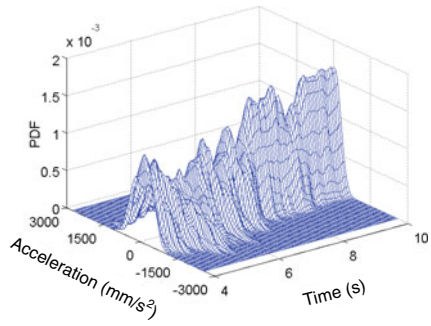

(a) probability density surface

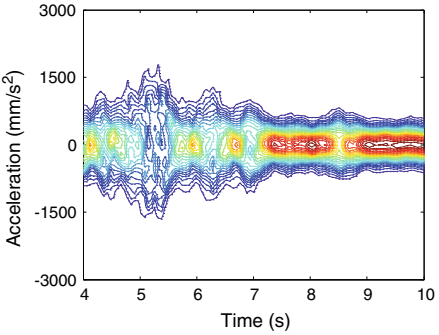

(b) probability density contour

Fig. 3.16 Probability density of structural acceleration at typical time interval

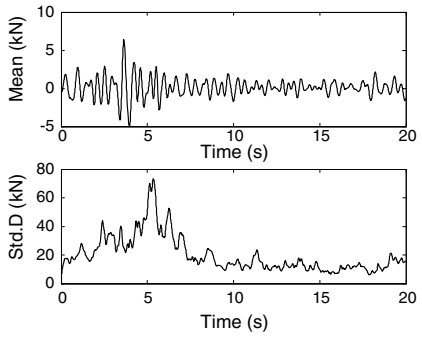

(a) mean and standard deviation

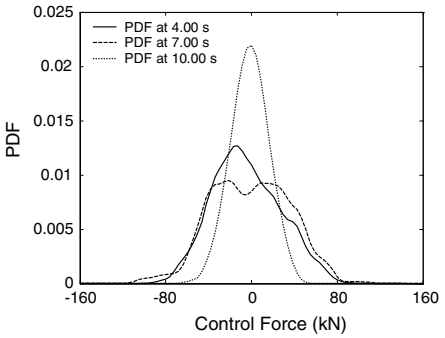

(b) probability density curves

Fig. 3.17 Mean and standard deviation of control force and PDFs at typical instants of time

1988). However, the generalized probability density evolution equation is essentially a nonlinear first-order partial differential equation, which results in the differences of PDFs between system state and control force even if the control force is linearly mapped from the system state.

3.4.2 Controlled Multiple-Story Building Structure

An eight-story shear frame attached with fully distributed active tendon systems is studied. The properties of the uncontrolled structure are taken from the publication by Yang et al. (Yang et al. 1987). The story mass is $m_i = 3.456 \times 10^5$ kg; interstory stiffness is $k_i = 3.404 \times 10^2$ kN/mm; and internal damping coefficient of each story is $c_i = 2.937$ kNs/mm, which corresponds to a 2% damping ratio for the first vibration mode of the entire structure. The external damping is assumed to be zero. The calculated natural frequencies are 5.79, 17.18, 27.98, 37.82, 46.38, 53.36, 58.53, and 61.69 rad/s, respectively. The constraint quantity, evaluation quantity, and control objective are the same as those of the case shown in Sect. 3.4.1. The quantile function is defined as the mean plus one time of standard deviation. The threshold of interstory drift is set as 15 mm. The random seismic ground motion model is employed, of which the peak ground acceleration is $0.3g$.

Figure 3.18 shows the relation between the mean, quantile of equivalent extreme-value displacement, equivalent extreme-value acceleration, equivalent extreme-value control force, and the ratio of coefficients of weighting matrices. It is shown that (i) as ratio $q/r \geq 4 \times 10^{13}$, the quantile of the displacement is completely within its threshold as a constraint; (ii) as ratio $q/r = 1 \times 10^{14}$, the standard deviation of the displacement is minimum and the mean approaches to its minimum, which are both decreasing significantly; and the mean of control force increases constantly, of which the standard deviation, however, provisionally possesses a small value. Therefore, it is reasonable to take the optimal ratio $q^*/r^* = 1 \times 10^{14}$; $q^* = 100$, $r^* = 10^{-12}$ in this numerical case.

Figure 3.19 shows the time histories of mean and standard deviation of the first and eighth interstory drifts with and without controls. It is seen that the interstory drifts are reduced significantly when the structure is under control. The amplitudes of interstory drifts with control are nearly 4 times smaller than those without control. Similar to the displacement of the single-story structural system with control shown in Sect. 3.4.1, the time interval with larger amplitudes gets an obvious improvement. The interstory drift with control exhibits almost same mitigation ratio along the story level of the structure. Story acceleration, however, does not exhibit this behavior. Shown in Fig. 3.20 is the time histories of the mean and standard deviation of the first and eighth story accelerations with and without controls. It is seen that the first story acceleration remains nearly unchanged; while the eighth story acceleration is improved significantly. The two story accelerations, however, have almost the same variation, owing to the fact that the objective of the stochastic optimal control is

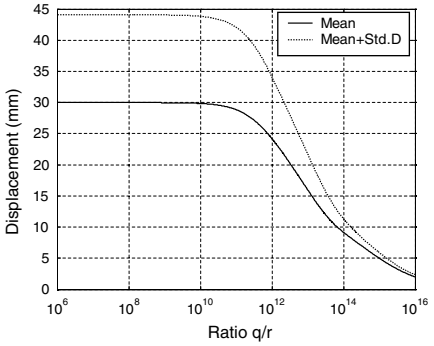

(a) equivalent extreme-value displacement

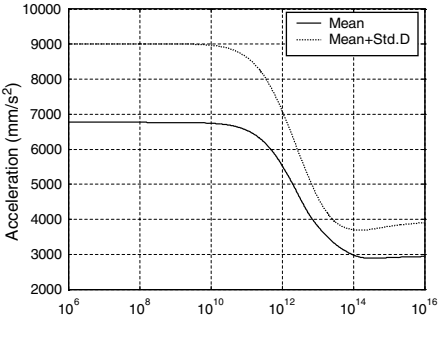

(b) equivalent extreme-value acceleration

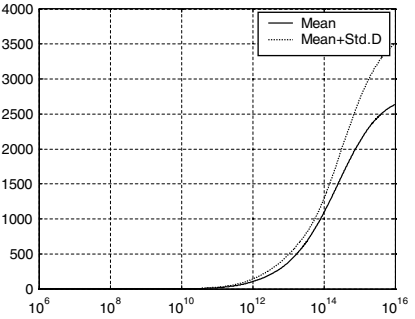

(c) equivalent extreme-value control force

Fig. 3.18 Relation between mean, quantile of quantities, and ratio of coefficients of weighting matrices

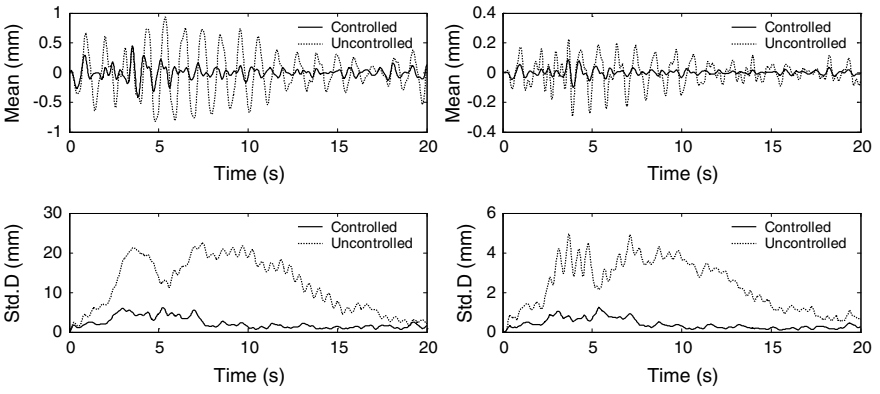

(a) 1st story (b) 8th story

Fig. 3.19 Time histories of mean and standard deviation of interstory drifts of structure with and without controls

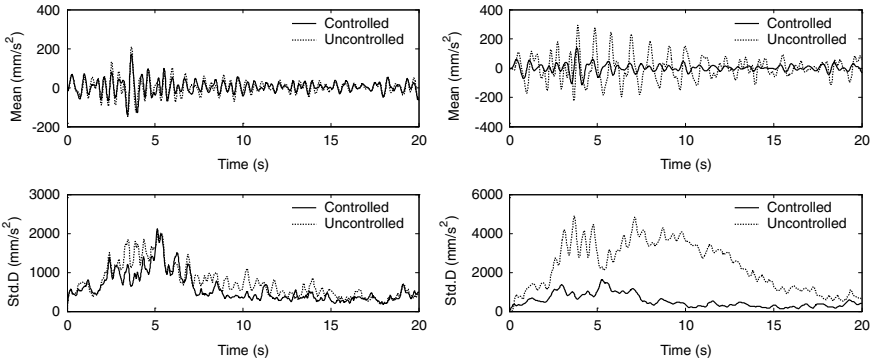

(a) 1st story (b) 8th story

Fig. 3.20 Time histories of mean and standard deviation of story accelerations of structure with and without controls

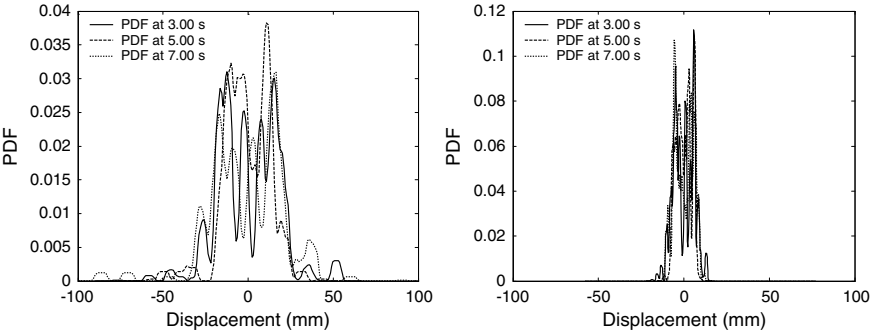

(a) without control (b) with control

Fig. 3.21 PDFs of first interstory drift at typical instants of time

to optimize the structural performance in the sense of the trade-off between system quantities of interest.

The PDFs of the first and eighth interstory drifts at typical instants of time 3 s, 5 s, and 7 s with and without controls are shown in Figs. 3.21 and 3.22. By comparison with the cases without control, the distribution range of the PDFs of interstory drifts with control becomes narrower and the shape of the PDFs arises to be more irregular. It is indicated that the shear frame structure with control does not move as a similar profile to that without control since the introduction of the control force leads to a change of contribution from vibrational modes to structural responses. Similar control effectiveness is shown in the PDFs of the first and eighth story accelerations at typical instants of time with and without controls; see Figs. 3.23 and 3.24. The probability densities of the first interstory drift and story acceleration at typical time interval from 3 s to 7 s are pictured in Figs. 3.25 and 3.26, respectively.

Time histories of the mean and standard deviation of the first and eighth interstory control forces are shown in Fig. 3.27. It is readily seen that the first interstory control

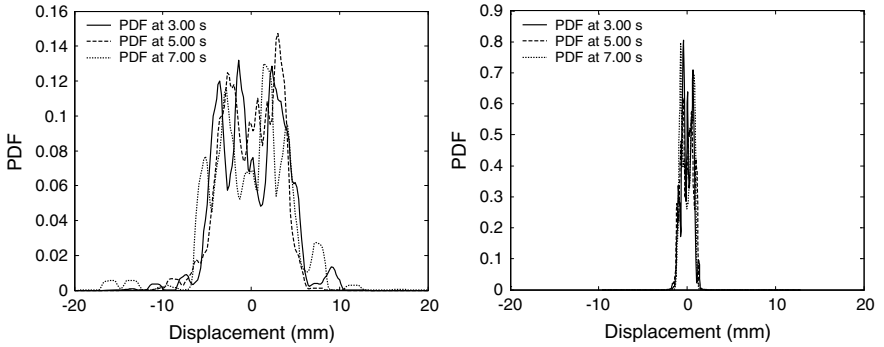

Fig. 3.22 PDFs of eighth interstory drift at typical instants of time

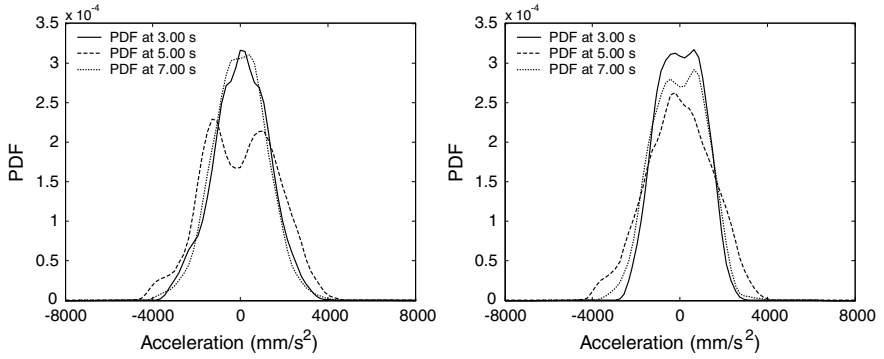

Fig. 3.23 PDFs of first story acceleration at typical instants of time

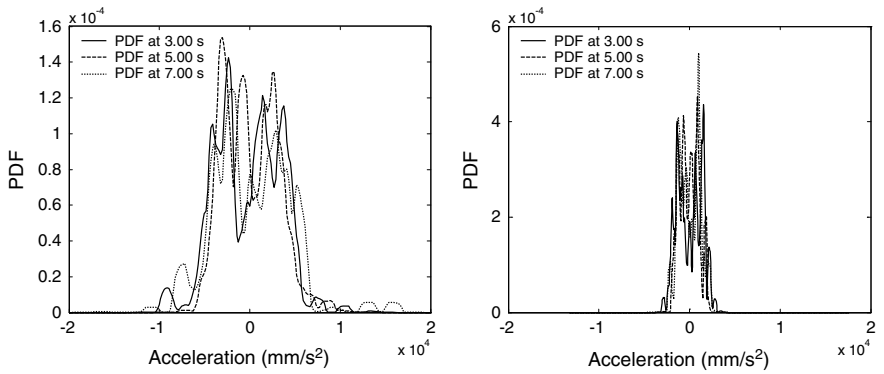

Fig. 3.24 PDFs of eighth story acceleration at typical instants of time

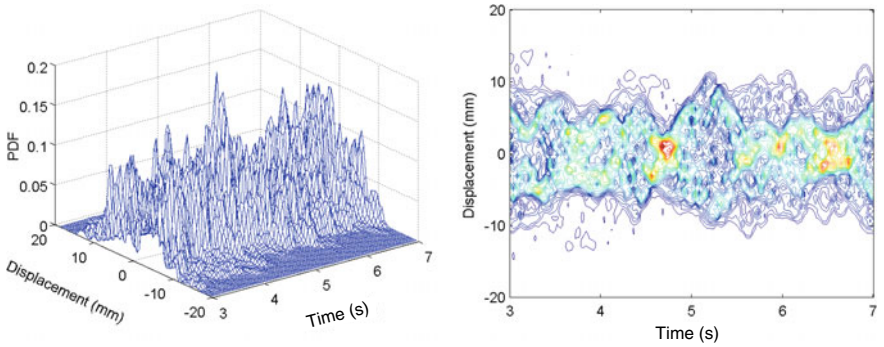

(a) probability density surface (b) probability density contour

Fig. 3.25 Probability density of first interstory drift at typical time interval with control

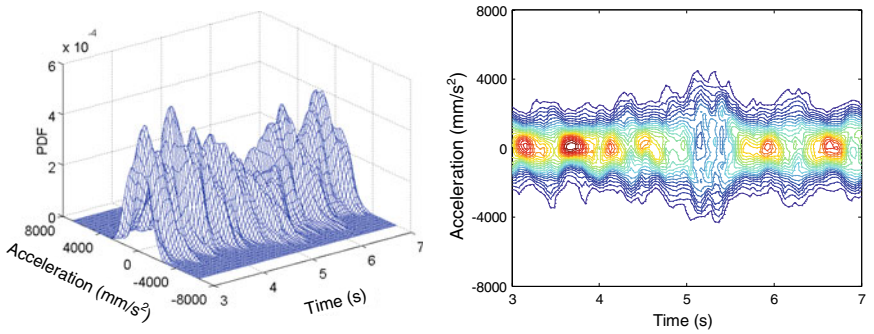

Fig. 3.26 Probability density of first story acceleration at typical time interval with control

force has certain similarities to the eighth interstory control force except the scale of amplitude, of which the first interstory control force is 10 times larger than the eighth interstory control force. It is also seen that the time histories of the standard deviations of the first and eighth interstory control forces exhibit positive similarities, while the time histories of the means exhibit negative similarities. In view of Figs. 3.19 and 3.20, one might recognize that the responses of the two stories arise to be asynchronous, and accordingly the feedback control forces on the two stories arise to be asynchronous. This phenomenon is also shown in the PDFs of interstory control forces at typical instants of time; see Fig. 3.28.

Control effectiveness of extreme-value responses of the eight-story building structure by active tendon systems is shown in Table 3.1. It is seen that the interstory drift reduces significantly, of which the mean decreases about 70%, the standard deviation decreases about 85%, and the amplitude of the response is reduced nearly the same along story level of the structure. The reduction of acceleration from the fifth story to the eighth story with control is remarkable as well, of which the mean decreases 50% on average and the standard deviation decreases 75% on average. It is noted

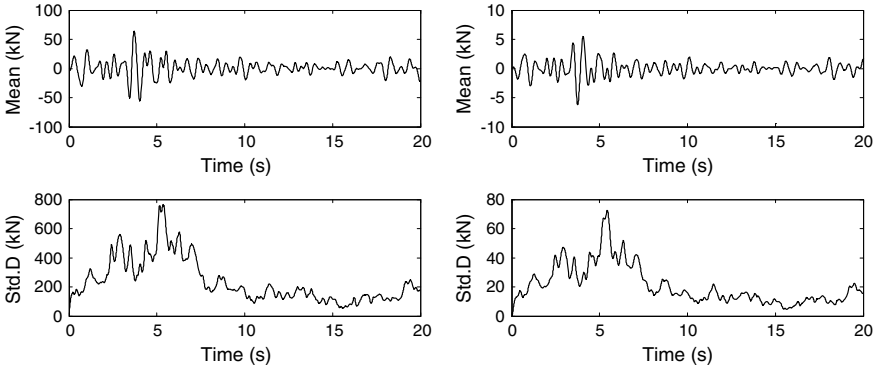

(a) 1st story (b) 8th story

Fig. 3.27 Time histories of mean and standard deviation of interstory control forces

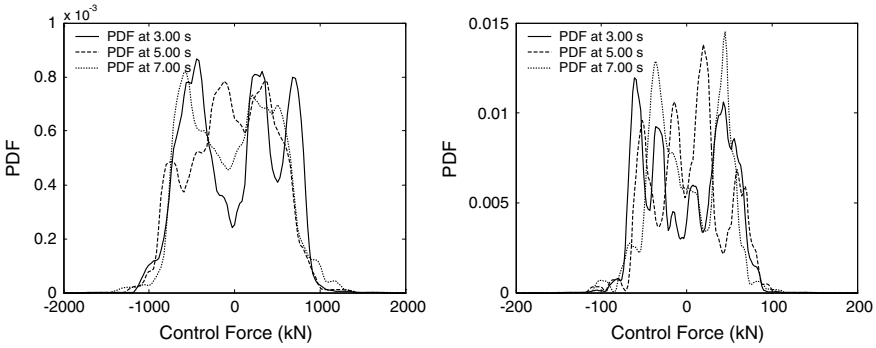

(a) 1st story (b) 8th story

Fig. 3.28 PDFs of interstory control forces at typical instants of time

that the control effectiveness of acceleration of the low two stories is obviously less than other stories. As it is indicated in Table 3.1, the story acceleration arises to be more uniform along the story level of the structure after the structure is controlled. Moreover, the higher the story level, the smaller the control force arises to be. Therefore, more control cost is required for the low stories in order to attain a uniform story acceleration along the story level. The ratios of extreme-value control forces, besides, between different interstories are almost equal to those of extreme-value interstory drift, which is due to the fact that the control force is a linear function with respect to the interstory drift.

Table 3.1 Control effectiveness of eight-story shear frame by active tendon systems

Equ. ext.-value			Story number							
			1	2	3	4	5	6	7	8
Interstory drift (mm)	Mn	Unc.	29.95	28.66	26.65	24.64	21.94	18.11	13.02	6.84
		Con.	9.17	8.62	7.97	7.14	6.12	4.86	3.39	1.74
		Eff.	−69.38%	−69.92%	−70.09%	−71.02%	−72.11%	−73.16%	−73.96%	−74.56%
	Std. d	Unc.	14.11	13.91	13.16	11.39	9.15	6.84	4.56	2.28
		Con.	2.16	2.05	1.85	1.61	1.32	1.02	0.69	0.35
		Eff.	−84.69%	−85.26%	−85.94%	−85.86%	−85.57%	−85.09%	−84.87%	−84.65%
Story acceleration (mm/s^2)	Mn	Unc.	3031.9	3489.5	4140	4547.7	4645	5150.4	6118.4	6759.5
		Con.	2803.3	2616.0	2435.8	2302.3	2229.7	2230.9	2264.0	2294.0
		Eff.	−7.54%	−25.03%	−41.16%	−49.37%	−52.00%	−56.68%	−63.00%	−66.06%
	Std. d	Unc.	918.0	1296.2	1549.7	1671.4	1976.6	2268.7	2249.2	2249.5
		Con.	862.3	693.1	526.5	405.6	376.1	410.8	455.3	483.6
		Eff.	−6.07%	−46.53%	−66.03%	−75.73%	−80.97%	−81.89%	−79.76%	−78.50%
Interstory control force (kN)	Mn		1090.25	712.66	503.30	339.16	205.52	131.26	117.39	99.49
	Std. d		196.63	155.79	142.61	127.91	102.72	62.04	29.67	21.58

[a]Effectiveness is defined as (Con.-Unc.)/Unc.

3.5 Comparative Studies against LQG

In order to validate the physically based stochastic optimal control, comparative studies against the classical LQG and the deterministic control are carried out. For illustrative purposes, the numerical example addressed in Sect. 3.4.1 is employed.

Concerning the controlled structure with active tendon system shown in Fig. 3.4, the equation of motion is given by

$$\ddot{x}(t) + 2\zeta\omega_0\dot{x}(t) + \omega_0^2 x(t) = m^{-1}u(t) - \ddot{x}_g(\boldsymbol{\Theta}, t) \tag{3.5.1}$$

which can be rewritten as a formulation in state space as follows:

$$\dot{\mathbf{Z}}(t) = \mathbf{A}\mathbf{Z}(t) + \mathbf{B}u(t) + \mathbf{D}\ddot{x}_g(\boldsymbol{\Theta}, t) \tag{3.5.2}$$

where

$$\mathbf{Z}(t) = \begin{bmatrix} x(t) \\ \dot{x}(t) \end{bmatrix}, \mathbf{A} = \begin{bmatrix} 0 & 1 \\ -\omega_0^2 & -2\zeta\omega_0 \end{bmatrix}, \mathbf{B} = \begin{bmatrix} 0 \\ m^{-1} \end{bmatrix}, \mathbf{D} = \begin{bmatrix} 0 \\ -1 \end{bmatrix} \tag{3.5.3}$$

The cost function of the LQG is defined as (Chen et al. 1998)

$$J_1(\mathbf{Z}, u) = E\left[\mathbf{S}(\mathbf{Z}(t_f), t_f) + \frac{1}{2}\int_{t_0}^{t_f} (\mathbf{Z}^{\mathrm{T}}(t)\mathbf{Q}_{\mathbf{Z}}\mathbf{Z}(t) + \mathbf{R}_{\mathbf{U}}u^2(t))\mathrm{d}t\right] \tag{3.5.4}$$

of which the constraint condition is given by

$$\begin{cases} \mathrm{d}\mathbf{Z}(t) = [\mathbf{A}\mathbf{Z}(t) + \mathbf{B}u(t)]\mathrm{d}t + \mathbf{L}\mathrm{d}w(t) \\ \mathbf{Z}(t_0) = \mathbf{0} \end{cases} \tag{3.5.5}$$

where $\mathbf{L}$ is the (2×1) matrix denoting the location of external excitation; $w(t)$ denotes the one-dimensional Brownian motion, which is generally modeled as a white Gaussian noise:

$$E[\mathrm{d}w(t)] = 0, E[\mathrm{d}w^2(t)] = 2\beta S_0\mathrm{d}t \tag{3.5.6}$$

where S_0 is the spectral intensity factor of random seismic ground motion $\ddot{x}_g(\boldsymbol{\Theta}, t)$, which is estimated by

$$S_0 = \frac{\bar{a}_{\max}^2}{f^2\omega_e} \tag{3.5.7}$$

where $\bar{a}_{\max}$ denotes the mean of the peak ground acceleration of random seismic ground motion; f denotes the peak factor; and ω_e denotes the spectral area pertain-

Table 3.2 Relation between spectral intensity factor, peak ground acceleration (PGA), and site class

Site class/PGA	I		II		III		IV	
	$0.11g$	$0.3g$	$0.11g$	$0.3g$	$0.11g$	$0.3g$	$0.11g$	$0.3g$
f	2.9	2.9	3.0	3.0	3.1	3.1	3.2	3.2
ω_e (rad s^{-1})	59.50	59.50	39.71	39.71	29.93	29.93	19.95	19.95
S_0 (m^2 s^{-3})	0.0023	0.0173	0.0033	0.0242	0.0040	0.0301	0.0057	0.0423

See Chinese Code for Seismic Design of Building Structures (GB50011-2010), $1g = 9.8$ m/s^2

ing to unit spectral intensity factor. Table 3.2 shows the spectral intensity factor in the cases of peak ground accelerations $\bar{a}_{\max} = 0.1g, 0.3g$ and typical site classes in accordance with the Chinese Code for Seismic Design of Building Structures (GB50011-2010).

It is seen that the mathematical formulation of the equation of motion of the controlled structure with active tendon system, i.e., Eq. (3.5.5) is just the classical Itô stochastic differential equation. As it is mentioned in the previous sections, the measurement noise inherent in system state and control force is out of concern, and is thus ignored in this study. The random seismic ground motion $\ddot{x}_g(\boldsymbol{\Theta}, t)$ is assumed to be a wide-band excitation and mathematically modeled by a nominal white Gaussian noise.

Transferring the constraint extreme-value problem of function Eq. (3.5.4) to an unconstraint extreme-value problem, the solution of the control system can be derived by solving Hamilton–Jacobi–Bellman equation in the context of randomness. Introducing a generalized Hamilton function as follows (Li and Chen 2009):

$$H[\mathbf{Z}^*(t), u(t), t] = \frac{1}{2}\left(\mathbf{Z}^{*\mathrm{T}}\mathbf{Q}_{\mathbf{Z}}\mathbf{Z}^* + \mathbf{R}_{\mathrm{U}}u^2\right) + \frac{\partial V}{\partial \mathbf{Z}}\left(\mathbf{A}\mathbf{Z}^* + \mathbf{B}u\right) + \pi S_0 \mathrm{Tr}\left(\frac{\partial^2 V}{\partial \mathbf{Z}^2}\mathbf{L}\mathbf{L}^{\mathrm{T}}\right) \tag{3.5.8}$$

where V denotes the optimal value function and is assumed to be

$$V(\mathbf{Z}(t), t) = \frac{1}{2}\mathbf{Z}^{\mathrm{T}}(t)\mathbf{P}(t)\mathbf{Z}(t) + \nu(t) \tag{3.5.9}$$

of which $\nu(t)$ is a correct term with respect to the randomness associated with the generalized Hamilton function.

Utilizing the dynamic programming method, one could gain the solution

$$u(t) = -\mathbf{R}_{\mathrm{U}}^{-1}\mathbf{B}^{\mathrm{T}}\mathbf{P}(t)\mathbf{Z}(t) \tag{3.5.10}$$

$$\nu(t) = -\pi S_0 \int_{t_0}^{t_f} \mathrm{Tr}(\mathbf{P}(t)\mathbf{L}\mathbf{L}^{\mathrm{T}})\mathrm{d}t \tag{3.5.11}$$

where $\mathbf{P}(t)$ denotes the Riccati matrix, satisfying with the matrix algebraic Riccati equation; see Eq. (3.3.17).

In view of Eqs. (3.5.10) and (3.3.18), the control law of the LQG has the same formulation to the LQR-based PSO for a closed-loop system in the sense of sample trajectory, and the so-called deterministic equivalence principle is satisfied. It is shown as well that concerning the linear time-invariant system subjected to the white Gaussian noise, the gain matrix can be calculated offline though the Hamilton function includes a random excitation term.

Substituting Eq. (3.5.10) into Eq. (3.5.1) and using the Fourier transform on both sides, one has

$$\{[(\omega_0^2 + m^{-1}\widehat{K}) - \omega^2] + (2\zeta\omega_0 + m^{-1}\widehat{C})(\mathrm{i}\omega)\}x(\omega) = -\ddot{x}_g(\boldsymbol{\Theta}, \omega) \tag{3.5.12}$$

where $\widehat{C}$, $\widehat{K}$ denote the numerical damping and numerical stiffness provided by the control force $u(t)$, respectively,

$$\widehat{C} = \mathbf{R}_{\mathbf{U}}^{-1}(B_1 P_{12} + B_2 P_{22}),\ \widehat{K} = \mathbf{R}_{\mathbf{U}}^{-1}(B_1 P_{11} + B_2 P_{21}) \tag{3.5.13}$$

According to the statistical relation between the input and output of linear stochastic systems in frequency domain (Crandall 1958), one has

$$S_X(\omega) = \frac{S_0}{[(\omega_0^2 + m^{-1}\widehat{K}) - \omega^2]^2 + (2\zeta\omega_0 + m^{-1}\widehat{C})^2\omega^2} \tag{3.5.14}$$

In view of Wiener–Khintchine theorem (Wiener 1964; Chatfield 1989), the mean-square displacement under control is then derived as follows:

$$E[x^2(t)] = \int_{-\infty}^{\infty} \frac{S_0}{[(\omega_0^2 + m^{-1}\widehat{K}) - \omega^2]^2 + (2\zeta\omega_0 + m^{-1}\widehat{C})^2\omega^2}\mathrm{d}\omega \tag{3.5.15}$$

Concerning the integral shown in Eq. (3.5.15), a closed solution can be attained by virtue of a class of specified rules (Roberts and Spanos 1990), which is given by

$$E[x^2(t)] = \frac{\pi S_0}{(2\zeta\omega_0 + m^{-1}\widehat{C})(\omega_0^2 + m^{-1}\widehat{K})} \tag{3.5.16}$$

Obviously, there is a linear relation between system state and control force in frequency domain, which is given as

$$u(\omega) = [-\widehat{C}(\mathrm{i}\omega) - \widehat{K}]x(\omega) \tag{3.5.17}$$

Then, the mean-square control force can be derived as follows:

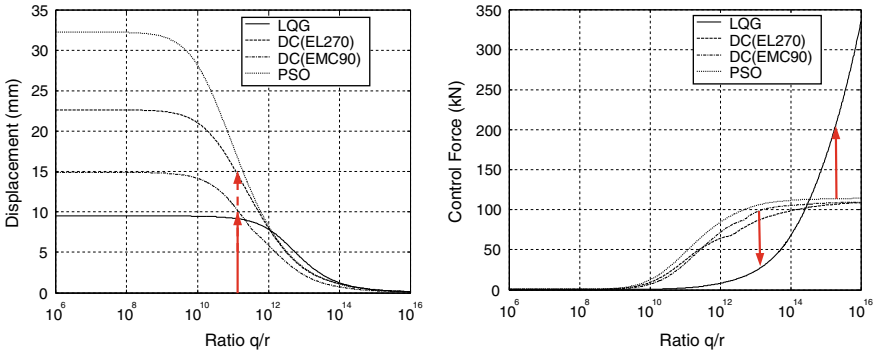

(a) structural displacement (b) control force

Fig. 3.29 Relation between root-mean-square quantities and ratio of coefficients of weighting matrices by means of PSO, LQG, and DC

$$E[u^2(t)] = \int_{-\infty}^{\infty} \frac{(\widehat{K}^2 + \widehat{C}^2\omega^2)S_0}{[(\omega_0^2 + m^{-1}\widehat{K}) - \omega^2]^2 + (2\zeta\omega_0 + m^{-1}\widehat{C})^2\omega^2} \mathrm{d}\omega \tag{3.5.18}$$

Using the rule shown in Eq. (3.5.16) once again, one has

$$E[u^2(t)] = \frac{\pi S_0[\widehat{C}^2(\omega_0^2 + m^{-1}\widehat{K}) + \widehat{K}^2]}{(2\zeta\omega_0 + m^{-1}\widehat{C})(\omega_0^2 + m^{-1}\widehat{K})} \tag{3.5.19}$$

Figure 3.29 shows the relation between root-mean-square quantities and the ratio of coefficients of weighting matrices by means of the physically based stochastic optimal (PSO) control, the LQG control, and the deterministic control (DC) using random seismic ground motion, white Gaussian noise, and recorded seismic ground motions, i.e., EL270 and EMC90, as the external excitation. In this case, the coefficient of state weighting matrix is set as 100. For the LQG, the root-mean-square quantities can be calculated directly from Eqs. (3.5.16) and (3.5.19); while for the PSO and the DC, the root-mean-square quantities are identified as their peaks since the derivations of these quantities are time variant and nonstationary.

It is indicated that (i) as the ratio $10^6 \leq q/r < 10^{12}$, the LQG underestimates the structural displacement, in that the stationary response of the structural system subjected to white Gaussian noise is several times lower than the peaks of the nonstationary response of the structural system subjected to the random and recorded seismic ground motions. The LQG, meanwhile, underestimates the desired control force. It is seen that the control force assessed by the LQG increases exponentially along with the ratio of coefficients of weighting matrices in logarithmic scale. The control force assessed by the PSO, however, increases logarithmically along with the ratio of coefficients of weighting matrices in logarithmic scale; (ii) as ratio

$10^{12} \leq q/r < 4 \times 10^{14}$, the structural displacement controlled by the PSO declines significantly and the peak is close to that controlled by the LQG. The difference of control forces between the two schemes becomes large along with the ratio of coefficients of weighting matrices in logarithmic scale; (iii) as ratio $q/r \geq 4 \times 10^{14}$, the structural responses controlled by the two schemes are almost the same, but the control force of the LQG increases exponentially and surpasses that of the PSO rapidly; and (vi) similar to the structural displacement, the structural velocity and structural acceleration quantified by the LQG change exponentially along with the ratio of coefficients of weighting matrices. In summary, the LQG underestimates the desired control force when the ratio of coefficients of weighting matrices is set at a low level, while it overestimates the desired control force when the ratio of coefficients of weighting matrices is set at a high level. It is thus remarked that employing the LQG with nominal white Gaussian noise as the input cannot attain a reasonable structural control system for civil engineering structures.

It is also seen from Fig. 3.29 that by means of the deterministic control (DC), the structural control system designed as the seismic ground motion EMC90 might be disabled when the structure is subjected to the seismic ground motion EL270. If the ratio of coefficients of weighting matrices is set as $q/r = 2 \times 10^{11}$, for instance, the extreme value of structural displacement is within 10 mm when the structure is subjected to the seismic ground motion EMC90. However, the structural displacement attains 15 mm when the structure is subjected to the seismic ground motion EL270, although the required control forces designed as the two recorded seismic ground motions are almost same. It is thus demonstrated that the deterministic control cannot guarantee a safe structure; while the PSO offers an elegant means for the logical control of structures that can secure a safe structure in the sense of probability.

3.6 Discussions and Summaries

The relevant theory and methods for the classical stochastic optimal control such as the LQG still remain open for the control gain design of engineering structures subjected to the nonstationary excitations, e.g., strong earthquakes and high winds. In essence, moreover, the classical stochastic optimal control belongs to a family of moment-based schemes. The physically based stochastic optimal control, however, facilitates the control gain design of engineering structures with strong nonlinearities and subjected to nonstationary excitations, which circumvents the dilemma pertaining to the classical stochastic optimal control. Moreover, the physically based stochastic optimal control can implement the regulation of probability density of structural systems, by virtue of the probabilistic criteria in terms of structural reliability for parameter optimization of control law. The reliability-based probabilistic criteria can be readily applied by the proposed control scheme since the PSO straightforwardly include the solution of probability density of structural responses provided by the probability density evolution method.

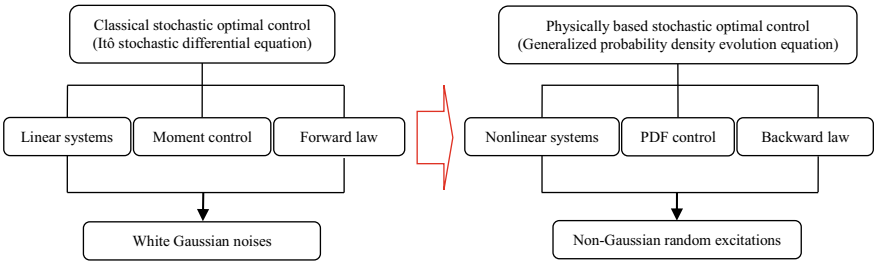

Fig. 3.30 Schematic diagram of differences between classical stochastic optimal control and PSO

Indeed, a probability-density-based stochastic optimal control can be implemented in conjunction with the classical Fokker–Planck–Kolmogorov equation (FPK equation). However, similar to the situation of the FPK equation in the field of random vibration, the FPK equation with control force term still encounters the challenge of solving the probability density of stochastic systems in practice. Applicability of the FPK equation-based stochastic optimal control is far less than the LQG though the latter merely concerns the second-order moment of structural responses. While the generalized probability density evolution equation involved in the PSO breaks through the dilemma, which forms into the logical basis for the theory and methods of stochastic optimal control of structures. A schematic diagram shows the differences between the classical stochastic optimal control and the PSO; see Fig. 3.30.

It is worth noting that the classical stochastic optimal control is capable of implementing the moment-based control and attaining probability-density-based control in cases of extremely particular situations through defining the FPK equation involving control force terms. However, the physically based stochastic optimal control is readily to implement the probability-density-based control by connecting two families of equations: one is the equation of motion of controlled stochastic systems, e.g., Eq. (3.2.1), which is termed as the physical equation; another is the probability density evolution equation of controlled stochastic systems, e.g., Eqs. (3.2.9) and (3.2.10), which is termed as the evolution equation. The solving of the physical equation is carried out over realizations, which resorts to advanced techniques employed in the deterministic optimal control, such as the linear quadratic regulator (LQR), the optimal polynomial control (OPC), etc. Most of these techniques are optimal control methods based on the Riccati equation and dynamic programming methods based on the Bellman's optimality principle.

References

Åström KJ (1970) Introduction to stochastic control theory. Academic Press, New York
Athans M, Falb P (1966) Optimal control: an introduction to the theory and its applications. McGraw Hill, New York

Bani-Hani KA, Alawneh MR (2007) Prestressed active post-tensioned tendons control for bridges under moving loads. Struct Control Health Monit 14:357–383
Bucy RS, Kalman RE (1961) New results in linear filtering and prediction theory. ASME Trans J Basic Eng 83:95–108
Chang CC, Yu LO (1998) A simple optimal pole location technique for structural control. Eng Struct 20(9):792–804
Chatfield C (1989) The analysis of time series-an introduction, 4th edn. Chapman and Hall, London
Chen JB, Li J (2008) Strategy for selecting representative points via tangent spheres in the probability density evolution method. Int J Numer Meth Eng 74(13):1988–2014
Chen JB, Liu WQ, Peng YB, Li J (2007) Stochastic seismic response and reliability analysis of base-isolated structures. J Earthq Eng 11(6):903–924.
Chen SP, Li XJ, Zhou XY (1998) Stochastic linear quadratic regulators with indefinite control weight costs. SIAM J Control Optim 36:1685–1702
Chung LL, Reinhorn AM, Soong TT (1988) Experiments on active control of seismic structures. ASCE J Eng Mech 114(2):241–256
Crandall SH (1958) Random vibration. Technology Press of MIT, Wiley, New York
Florentin JJ (1961) Optimal control of continuous time, Markov, stochastic systems. J Electron Control 10:473–488
Ho CC, Ma CK (2007) Active vibration control of structural systems by a combination of the linear quadratic Gaussian and input estimation approaches. J Sound Vib 301:429–449
Josa-Fombellida R, Rincón-Zapatero JP (2007) New approach to stochastic optimal control. J Optimiz Theory and App 135(1):163–177
Kalman RE (1960a) On the general theory of control systems. In: Proceedings of 1st IFAC Moscow congress. Butterworth Scientific Publications
Kalman RE (1960b) A new approach to linear filtering and prediction problems. ASME Trans J Basic Eng 82:35–45
Kohiyama M, Yoshida M (2014) LQG design scheme for multiple vibration controllers in a data center facility. Earthq Struct 6(3):281–300
Kushner HJ (1962) Optimal stochastic control. IRE Trans Autom Control AC-7:120–122
Li J, Ai XQ (2006) Study on random model of earthquake ground motion based on physical process. Earthq Eng Eng Vib 26(5):21–26 (in Chinese)
Li J, Chen JB (2008) The principle of preservation of probability and the generalized density evolution equation. Struct Saf 30:65–77
Li J, Chen JB (2009) Stochastic dynamics of structures. Wiley, Singapore
Li J, Chen JB, Fan WL (2007) The equivalent extreme-value event and evaluation of the structural system reliability. Struct Saf 29(2):112–131
Li J, Liu ZJ (2006) Expansion method of stochastic processes based on normalized orthogonal bases. J Tongji Univ (Nat Sci) 34(10):1279–1283 (in Chinese)
Li J, Peng YB, Chen JB (2010) A physical approach to structural stochastic optimal controls. Probabilistic Eng Mech 25(1):127–141
Lin YK, Cai GQ (1995) Probabilistic structural dynamics: advanced theory and applications. McGraw-Hill, New York
Mathews JH Fink KD (2003) Numerical methods Using Matlab, 4th edn. Prentice-Hall
Øksendal B (2005) Stochastic differential equations: An introduction with applications, 6th edn, Springer-Verlag, Berlin
Roberts JB, Spanos PD (1990) Random vibration and statistical linearization. Wiley, West Sussex
Soong TT (1990) Active structural control: theory and practice. Longman Scientific & Technical, New York
Stengel RF (1986) Stochastic optimal control: theory and application. Wiley, New York
Stengel RF, Ray LR, Marrison CI (1992) Probabilistic evaluation of control system robustness. In: IMA workshop on control systems design for advanced engineering systems: complexity, uncertainty, information and organization, Minneapolis, MN
Sun JQ (2006) Stochastic dynamics and control. Elsevier, Amsterdam

Wiener N (1949) Extrapolation, interpolation and smoothing of stationary time series, with engineering applications. The MIT Press, Cambridge
Wiener N (1964) Time series. The MIT Press, Cambridge
Yang JN (1975) Application of optimal control theory to civil engineering structures. ASCE J Eng Mech Div 101(EM6):819–838
Yang JN, Akbarpour A, Ghaemmaghami P (1987) New optimal control algorithms for structural control. ASCE J Eng Mech 113(9):1369–1386
Yang JN, Li Z, Vongchavalitkul S (1994) Generalization of optimal control theory: linear and nonlinear control. ASCE J Eng Mech 120(2):266–283
Zhang WS, Xu YL (2001) Closed form solution for along-wind response of actively controlled tall buildings with LQG controllers. J Wind Eng Ind Aerodyn 89:785–807
Zhu WQ (2006) Nonlinear stochastic dynamics and control in Hamiltonian formulation. ASME Trans 59:230–248
Zhu WQ, Ying ZG, Soong TT (2001) An optimal nonlinear feedback control strategy for randomly excited structural systems. Nonlinear Dyn 24:31–51